# Structural Nonequilibrium Forces in Driven Colloidal Systems

Nico C. X. Stuhlmüller, Tobias Eckert, Daniel de las Heras,* and Matthias Schmidt†
*Theoretische Physik II, Physikalisches Institut, Universität Bayreuth, D-95440 Bayreuth, Germany*

(Received 22 December 2017; revised manuscript received 13 July 2018; published 31 August 2018)

We identify a structural one-body force field that sustains spatial inhomogeneities in nonequilibrium overdamped Brownian many-body systems. The structural force is perpendicular to the local flow direction, it is free of viscous dissipation, it is microscopically resolved in both space and time, and it can stabilize density gradients. From the time evolution in the exact (Smoluchowski) low-density limit, Brownian dynamics simulations, and a novel power functional approximation, we obtain a quantitative understanding of viscous and structural forces, including memory and shear migration.

DOI: 10.1103/PhysRevLett.121.098002

It is a very significant challenge of statistical physics to rationalize and predict nonequilibrium structure formation from a microscopic starting point. Primary examples include shear banding [1–3], where spatial regions of different shear rates coexist, and laning transitions in oppositely driven colloids [4,5], where regions of different flow direction occur, as well as migration effects in inhomogeneous shear flow [6–11]. In computer simulations, discriminating true steady states from slow initial transients can be difficult [12,13]. Often the nonequilibrium structuring effects have associated long timescales and strong correlations [14,15]. The underlying equilibrium phase diagram and bulk structure might already be complex and interfere with the genuine nonequilibrium effects [16,17].

To identify commonalities of all of the above situations, we investigate here a representative model situation. We put forward a systematic classification of the occurring nonequilibrium forces and identify a structural force component, which is able to sustain density gradients without creating dissipation. The structural force is solely due to the interaction between the particles, and it is hence of a nature different than that of the lift forces in hydrodynamics. We rationalize our findings by constructing an explicit power functional approximation (15) below.

We restrict ourselves to overdamped Brownian dynamics and consider the microscopically resolved position- and time-dependent one-body density $\rho(\mathbf{r},t)$ and one-body current $\mathbf{J}(\mathbf{r},t)$. Both fields are related via the (exact) continuity equation $\partial\rho/\partial t = -\nabla\cdot\mathbf{J}$; here $\nabla$ indicates the derivative with respect to position $\mathbf{r}$. The velocity profile is simply the ratio $\mathbf{v}(\mathbf{r},t) = \mathbf{J}(\mathbf{r},t)/\rho(\mathbf{r},t)$.

The exact time evolution, with no hydrodynamic interactions present, can then be expressed by the one-body force balance equation

$$\gamma\mathbf{v} = \mathbf{f}_{\rm int} + \mathbf{f}_{\rm ext} - k_BT\nabla\ln\rho, \tag{1}$$

where $\gamma$ is the single-particle friction constant against the (implicit) solvent, $\mathbf{f}_{\rm int}(\mathbf{r},t)$ is the internal force field, $\mathbf{f}_{\rm ext}(\mathbf{r},t)$ is a one-body external force field that, in general, drives the system out of equilibrium, and $-k_BT\nabla\ln\rho(\mathbf{r},t) \equiv \mathbf{f}_{\rm aid}(\mathbf{r},t)$ is the adiabatic ideal gas contribution due to the free thermal diffusion; here $k_B$ is the Boltzmann constant and $T$ is absolute temperature. The internal force field $\mathbf{f}_{\rm int}(\mathbf{r},t)$ arises from the interparticle interaction potential $u(\mathbf{r}^N)$, where $\mathbf{r}^N \equiv \mathbf{r}_1,\ldots,\mathbf{r}_N$ denotes the set of all position coordinates, and it can be expressed as an average over the interparticle one-body force density "operator"

$$\hat{\mathbf{F}}_{\rm int} = -\sum_i \delta(\mathbf{r}-\mathbf{r}_i)\nabla_i u(\mathbf{r}^N), \tag{2}$$

where the sum is over all particles, $\delta(\cdot)$ indicates the Dirac distribution, and $\nabla_i$ denotes the derivative with respect to $\mathbf{r}_i$. Using the probability distribution $\Psi(\mathbf{r}^N,t)$ of finding microstate $\mathbf{r}^N$ at time $t$, the average is built according to

$$\mathbf{f}_{\rm int}(\mathbf{r},t) = \rho(\mathbf{r},t)^{-1}\int d\mathbf{r}^N\Psi(\mathbf{r}^N,t)\hat{\mathbf{F}}_{\rm int}, \tag{3}$$

where the normalization is performed using the time-dependent one-body density, defined as the average

$$\rho(\mathbf{r},t) = \int d\mathbf{r}^N\Psi(\mathbf{r}^N,t)\hat{\rho}, \tag{4}$$

where $\hat{\rho} = \sum_i\delta(\mathbf{r}-\mathbf{r}_i)$ is the density operator.

The internal force field (3) can be further systematically decomposed [18,19] into adiabatic excess ($\mathbf{f}_{\rm axc}$) and superadiabatic one-body contributions ($\mathbf{f}_{\rm sup}$), according to

$$\mathbf{f}_{\rm int} = \mathbf{f}_{\rm axc} + \mathbf{f}_{\rm sup}. \tag{5}$$

 

Here the excess (over ideal gas) adiabatic force field $\mathbf{f}_{\rm axc}$ is the internal force field in a hypothetical equilibrium system that has the same density profile as the real nonequilibrium system at time $t$. Hence,

$$\mathbf{f}_{\rm axc}(\mathbf{r},t)=\rho(\mathbf{r},t)^{-1}\int d\mathbf{r}^N\Psi_{{\rm ad},t}(\mathbf{r}^N)\hat{\mathbf{F}}_{\rm int}, \tag{6}$$

where the average is over a canonical equilibrium distribution $\Psi_{{\rm ad},t}(\mathbf{r}^N)$ for the (unchanged) interparticle interaction potential $u(\mathbf{r}^N)$, but under the influence of a hypothetical external ("adiabatic") one-body potential $V_{{\rm ad},t}(\mathbf{r})$, which is constructed in order to yield in equilibrium the same one-body density as occurs in the dynamical system at time $t$ [18,19], i.e.,

$$\rho(\mathbf{r},t)=\rho_{{\rm ad},t}(\mathbf{r})\equiv\int d\mathbf{r}^N\Psi_{{\rm ad},t}(\mathbf{r}^N)\hat{\rho}. \tag{7}$$

The excess adiabatic force field is hence uniquely specified by (6) and (7); computer simulations permit direct access [19]. The force splitting (5) then defines the superadiabatic force field.

Here we demonstrate that $\mathbf{f}_{\rm sup}(\mathbf{r},t)$ further splits naturally and systematically into different contributions, which correspond to different physical effects. We have shown before that $\mathbf{f}_{\rm sup}(\mathbf{r},t)$ contains viscous force contributions [20]. These are of dissipative nature in that they work against the colloidal motion (i.e., antiparallel to the flow direction). Here we focus on the component of the superadiabatic force, which is perpendicular to the local flow direction $\mathbf{e}_v(\mathbf{r},t)$, where $\mathbf{v}=|\mathbf{v}|\mathbf{e}_v$; note that also $\mathbf{J}\|\mathbf{e}_v$. We hence define the (normal) structural force field $\mathbf{f}^{\perp}_{\rm sup}(\mathbf{r},t)$ as the component perpendicular to the local flow direction,

$$\mathbf{f}^{\perp}_{\rm sup}=\mathbf{f}_{\rm sup}-\mathbf{f}_{\rm sup}\cdot\mathbf{e}_v\mathbf{e}_v. \tag{8}$$

In contrast to the viscous force, the structural force is nondissipative, since the associated power density vanishes identically everywhere, $\mathbf{J}\cdot\mathbf{f}^{\perp}_{\rm sup}=|\mathbf{J}|\mathbf{e}_v\cdot\mathbf{f}^{\perp}_{\rm sup}=0$.

The structural force plays a vital role in nonequilibrium, as it can stabilize density gradients. In order to demonstrate this effect, we consider a two-dimensional toy system of Gaussian core particles [21] in an inhomogeneous external shear field. The pair interaction potential is $\epsilon\exp(-r^2/\sigma^2)$, where $r$ is the distance between both particles, and $\epsilon>0$ is the energy cost at zero separation. We use $\epsilon$ and $\sigma$ as the energy and the length scale, respectively. $N$ particles are located in a square box of length $L$ with periodic boundary conditions and (unit vector) directions $\mathbf{e}_x$ and $\mathbf{e}_y$ along the square box. The driving occurs along $\mathbf{e}_x$ according to an inhomogeneous external shear field,

$$\mathbf{f}_{\rm ext}(y,t)=f_0\sin(2\pi y/L)\theta(t)\mathbf{e}_x, \tag{9}$$

where $f_0$ is a constant that controls the magnitude of the driving force, and $\theta(\cdot)$ indicates the Heaviside (step) function, such that the force is instantaneously switched on at time $t=0$. Ultimately, the system reaches a steady state with a density gradient along $\mathbf{e}_y$, i.e., $\rho(\mathbf{r},\infty)=\rho(y)$, as we will see below. The density gradient is then solely sustained by the structural force $\mathbf{f}^{\perp}_{\rm sup}$.

In order to study the system on the Fokker-Planck level, we solve numerically the exact many-body Smoluchowski equation (SE) for overdamped Brownian motion. The time evolution of the probability distribution $\Psi$ is given exactly by the many-body continuity equation

$$\frac{\partial\Psi(\mathbf{r}^N,t)}{\partial t}=-\sum_i\nabla_i\cdot\mathbf{v}_i\Psi(\mathbf{r}^N,t). \tag{10}$$

where $\mathbf{v}_i$ is the velocity of particle $i$, given by the force balance

$$\gamma\mathbf{v}_i=-\nabla_i[u(\mathbf{r}^N)+k_BT\ln\Psi(\mathbf{r}^N,t)]+\mathbf{f}_{\rm ext}(\mathbf{r}_i,t). \tag{11}$$

We solve (10) and (11) numerically using a (standard) operator splitting approach [22]. Each spatial coordinate is discretized in increments $\Delta x=\sigma/5$; we use a time step $\Delta t/\tau=5\times10^{-3}$ with timescale $\tau=\sigma^2\gamma/\epsilon$. This method provides exact results of the nonequilibrium dynamics up to numerical inaccuracies. For $d$ space dimensions, the dimension of configuration space is $Nd$, which limits the applicability of the method to systems with small numbers of particles. Here, we consider $N=2$ in $d=2$, which renders the numerical field $Nd=4$ dimensional; hence, including time, we solve a $4+1$-dimensional numerical problem. As we show, despite the limited number of particles, all relevant forces are present.

In order to analyze larger systems, we use Brownian dynamics (BD), i.e., integrating in time the Langevin equation of motion, which corresponds to (10) and (11),

$$\gamma\frac{d\mathbf{r}_i(t)}{dt}=-\nabla_iu(\mathbf{r}^N)+\mathbf{f}_{\rm ext}(\mathbf{r}_i,t)+\boldsymbol{\chi}_i(t), \tag{12}$$

where $\boldsymbol{\chi}_i$ is a delta-correlated Gaussian random force. We use a time step $dt/\tau=10^{-4}$ and histogram bins of size $\Delta x=\sigma/20$. Density and force density profiles are obtained by averaging over a total time of $\sim10^9\tau$ in steady state.

In both SE and BD we use the iterative scheme of Refs. [19,23] to construct the adiabatic external potential $V_{{\rm ad},t}(\mathbf{r})$. The superadiabatic force then follows immediately from (5) since both $\mathbf{f}_{\rm int}$ and $\mathbf{f}_{\rm axc}$ can be directly calculated (sampled) in SE (BD). We have used the recently developed force sampling method [24] to improve the sampling of the density profile in BD. We expect, on principal grounds, that the SE and BD results agree (for identical values of system size and particle number, here $N=2$).

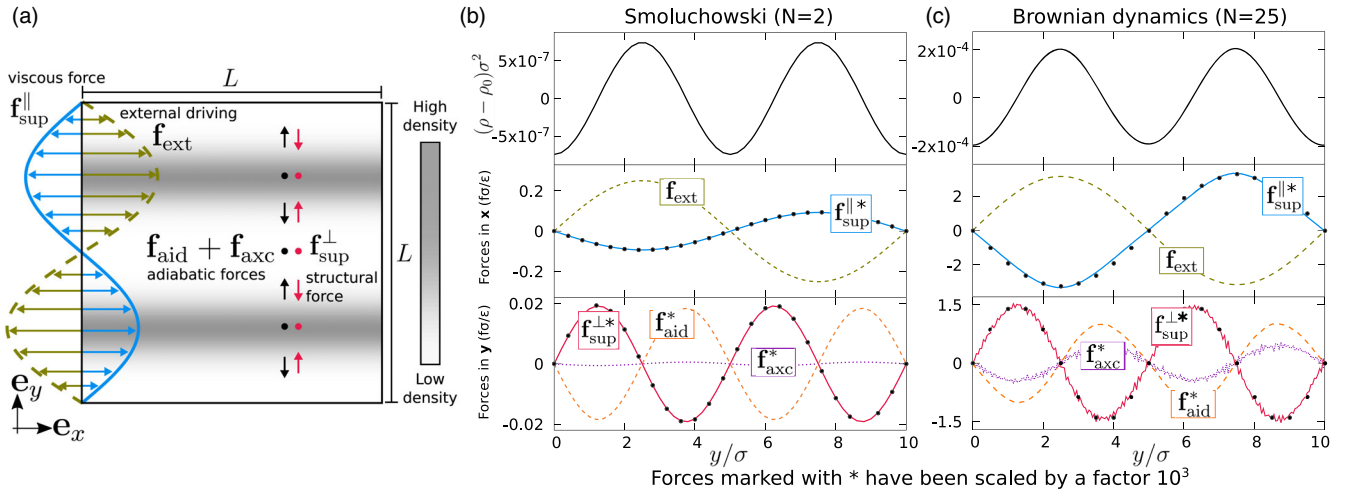


FIG. 1. (a) Illustration of the setup of a sinusoidal inhomogeneous shear flow induced by the external force field (9). Shown are the superadiabatic viscous force, which opposes the externally induced flow, the adiabatic excess, and ideal forces, which tend to relax the density gradient, as well as the superadiabatic structural nonequilibrium force, which restores the force balance in the $y$ direction. (b) Steady-state density and force profiles obtained by numerically solving the Smoluchowski equation in a system with $N = 2$, $L/\sigma = 10$, and $k_BT/\epsilon = 0.4$. (Top) Density profile for average density $\rho_0 = N/L^2 = 0.02\sigma^{-2}$ as a function of $y$. (Middle) Forces acting along $\mathbf{e}_x$ as a function of $y$: external force $\mathbf{f}_{\rm ext}$ of imposed amplitude $f_0 \approx 0.25\epsilon/\sigma$ (green dashed line) and superadiabatic viscous force (solid blue line) $\mathbf{f}^{\parallel}_{\rm sup}$. (Bottom) Forces acting along $\mathbf{e}_y$ as a function of $y$: adiabatic ideal (diffusion) $\mathbf{f}_{\rm aid}$ (orange dashed line), adiabatic excess $\mathbf{f}_{\rm axc}$ (violet dotted line), and superadiabatic structural force $\mathbf{f}^{\perp}_{\rm sup}$ (solid red line). (c) Same as (b) but for a system with $N = 25$, $L/\sigma = 10$, $\rho_0 = 0.25\sigma^{-2}$, $k_BT/\epsilon = 1$, and $f_0 \approx 3.14\epsilon/\sigma$. Data obtained using BD simulations. Forces marked with an asterisk in (b) and (c) have been multiplied by $10^3$ for clarity. The black circles in (b) and (c) indicate the theoretical prediction (18) of the superadiabatic viscous and structural forces.

A schematic showing all forces in steady state is shown in Fig. 1(a). The stationary density and force profiles obtained by solving the Smoluchowski equation ($N = 2$) and using BD simulations ($N = 25$) are shown in Figs. 1(b) and 1(c), respectively. A net flow exists along $+\mathbf{e}_x$ for $y < L/2$, since the external force is only partially balanced by a superadiabatic force of viscous nature $\mathbf{f}^{\parallel}_{\rm sup}$ along $-\mathbf{e}_x$ (see middle panels). Hence, in this situation, $\mathbf{e}_v = \mathbf{e}_x$. The viscous force has roughly the same shape as the external force but with reversed direction. The inhomogeneous external force (9) $\mathbf{f}_{\rm ext}(y)$ creates a density gradient in $\mathbf{e}_y$ (see top panels), since the particles migrate to the low shear rate regions. The adiabatic ideal (i.e., diffusive) and adiabatic excess (i.e., due to internal interaction) forces act along $\mathbf{e}_y$ and both try to relax the density gradient (see bottom panels). Both adiabatic forces are, however, exactly balanced by a structural superadiabatic force $\mathbf{f}^{\perp}_{\rm sup}$. The presence of the structural force hence renders the inhomogeneities of the density profile stationary in time.

We next analyze the system more systematically by comparing the behavior of the structural force to that of the viscous force. We show in Fig. 2(a) the amplitudes of the viscous force $\hat{f}^{\parallel}_{\rm sup}$ and the structural force $\hat{f}^{\perp}_{\rm sup}$ (measured from maximum to baseline) as a function of the amplitude of the external driving $f_0$. For small driving, the viscous force scales linearly with $f_0$. This behavior is expected, since for weak driving the velocity is proportional to the strength of the driving and the viscous force is proportional to the velocity (Newtonian rheology). The structural force, on the other hand, scales quadratically with $f_0$ and hence also with the velocity in the small driving regime. Both forces saturate for high values of $f_0$ [see the inset in Fig. 2(a)]. Figure 2(b) shows $\hat{f}^{\parallel}_{\rm sup}$ and $\hat{f}^{\perp}_{\rm sup}$ as a function of the average density $\rho_0$, revealing again profound differences between viscous and structural forces. The viscous force increases linearly with increasing $\rho_0$ at low densities and it saturates at high densities. In contrast, the structural force is nonmonotonic and exhibits a maximum at an intermediate density.

We rationalize these findings by developing a theory within the power functional approach [18]. Here the adiabatic and the superadiabatic contributions to the internal force field (5) are obtained via functional differentiation of two generating functionals,

$$\mathbf{f}_{\rm axc}(\mathbf{r}, t) = -\nabla \frac{\delta F_{\rm exc}[\rho]}{\delta \rho(\mathbf{r}, t)}, \tag{13}$$

$$\mathbf{f}_{\rm sup}(\mathbf{r}, t) = -\frac{\delta P^{\rm exc}_t[\rho, \mathbf{J}]}{\delta \mathbf{J}(\mathbf{r}, t)}. \tag{14}$$

Here $F_{\rm exc}[\rho]$ is the intrinsic excess (over ideal) Helmholtz equilibrium free energy functional of density functional theory, and $P^{\rm exc}_t[\rho, \mathbf{J}]$ is the excess (again over ideal)

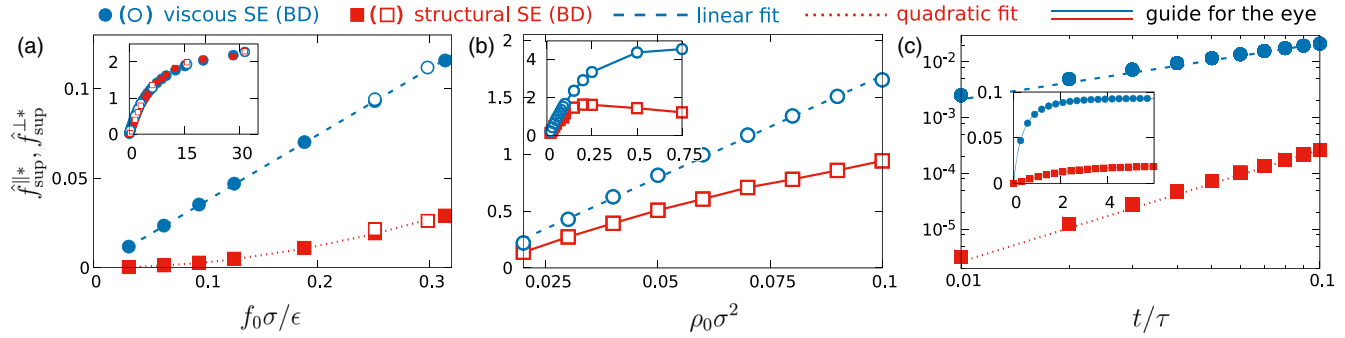


FIG. 2. Scaled amplitude of the superadiabatic forces $\hat{f}^{\alpha *}_{\rm sup} = 10^3 \hat{f}^{\alpha}_{\rm sup}\sigma/\epsilon$ with $\alpha \in \{\parallel, \perp\}$, as a function of (a) the amplitude of the external driving force $f_0$, (b) the average density $\rho_0 = N/L^2$, and (c) the time $t$. (a) Results for $L/\sigma = 10$, $N = 2$, and $k_BT/\epsilon = 0.4$. (b) Results in a system with $L/\sigma = 10$, $f_0 \approx 3.14\epsilon/\sigma$, $k_BT/\epsilon = 1$, and varying $N$. (c) Note the logarithmic scale in the main plot. The external driving force is switched on at $t = 0$. Results for $L/\sigma = 10$, $N = 2$, $k_BT/\epsilon = 0.4$, and $f_0 \approx 0.25\epsilon/\sigma$. In all panels, the viscous (structural) superadiabatic force is represented with blue circles (red squares), as indicated in the upper legend. Full (empty) symbols correspond to SE (BD) calculations. The blue dashed (red dotted) line indicates a linear (quadratic) fit to the data, as detailed in the Supplemental Material [25]. Solid lines are guides to the eye. The inset in each figure shows a linear plot of the same quantities as those in the main plot, but over an extended region.

superadiabatic functional of power functional theory [18]. Dynamical density functional theory (DDFT) [26–28] is obtained by setting $P^{\rm exc}_t = 0$; hence, no superadiabatic forces (neither viscous nor structural) occur in DDFT. In Ref. [20], using a change of variables in power functional theory from the current $\mathbf{J}$ to the velocity gradient $\nabla\mathbf{v}$, it is shown that the excess superadiabatic functional can be represented as a functional of $\nabla\mathbf{v}$. Following the same line, we consider a temporally non-Markovian but spatially local form,

$$P^{\rm exc}_t = \int d\mathbf{r}\left(\int_0^t dt' n_{tt'}(\nabla\times\mathbf{v})\cdot(\nabla\times\mathbf{v}') - \int_0^t dt'\int_0^t dt'' m_{tt't''}(\nabla\cdot\mathbf{v})(\nabla\times\mathbf{v}')\cdot(\nabla\times\mathbf{v}'')\right), \tag{15}$$

where we have used the shorthand notation $\mathbf{v}' = \mathbf{v}(\mathbf{r}, t')$ and $\mathbf{v}'' = \mathbf{v}(\mathbf{r}, t'')$. The factors $n_{tt'}$ and $m_{tt't''}$ are density-dependent temporal convolution kernels; the subscripts indicate the time arguments. Here the dependence is on the differences $t - t'$ and $t - t''$; the specific form of the kernels will depend on the form of the interparticle interaction potential $u(\mathbf{r}^N)$. In (15), we have left away bilinear and higher contributions in $\nabla\cdot\mathbf{v}$ [20]; these are important for compressional flow, but not for the present shear setup. Furthermore, as $\rho$ is practically constant in the cases considered, contributions in $\nabla\rho$ have also been omitted.

The superadiabatic force field is then obtained by inserting (15) into (14), where the derivative is carried out at fixed density, and hence $\delta/\delta\mathbf{J} = \rho^{-1}\delta/\delta\mathbf{v}$. Furthermore, the spatial derivatives in (15) can be suitably rearranged by (spatial) integration by parts. The resulting force density is

$$\rho\mathbf{f}_{\rm sup}(\mathbf{r}, t) = \int_0^t dt'\nabla\cdot n_{tt'}\nabla\mathbf{v}' - \int_0^t dt'\int_0^t dt''\nabla m_{tt't''}(\nabla\times\mathbf{v}')\cdot(\nabla\times\mathbf{v}''). \tag{16}$$

In steady state and for the case of constant density profile, (16) reduces to

$$\rho\mathbf{f}_{\rm sup}(\mathbf{r}) = \eta\nabla^2\mathbf{v} - \chi\nabla(\nabla\times\mathbf{v})^2, \tag{17}$$

where the prefactors $\eta = \lim_{t\to\infty}\int_0^t dt' n_{tt'}$ and $\chi = \lim_{t\to\infty}\int_0^t dt'\int_0^t dt'' m_{tt't''}$ are moments of the convolution kernels, which depend on the overall density. We can identify $\eta$ with the shear viscosity [20], such that the first term in (17) represents the viscous force. From carrying out the normal projection (8), the second contribution in (17) yields the structural force $\mathbf{f}^{\perp}_{\rm sup}(\mathbf{r}, t)$. Note that, while the forms (16) and (17) could possibly be postulated based on symmetry considerations alone, in the current framework, the generator (15) constitutes the more fundamental object, as the form of the force field follows via the functional derivative (14). Note that for the ideal gas ($u = 0$) $P^{\rm exc}_t = 0$ and $\mathbf{f}_{\rm sup} = 0$ by construction [18].

In accordance with our numerical results, we assume that the flow field is dominated by the external force; hence, we approximate (1) by $\mathbf{v}(y, t) \approx \mathbf{f}_{\rm ext}(y, t)/\gamma$. Insertion of (9) into (17) then yields

$$\mathbf{f}_{\rm sup}(y) = -\frac{f_0\eta k^2}{\gamma\rho}\sin(ky)\mathbf{e}_x + \frac{f_0^2\chi k^3}{\gamma\rho}\sin(2ky)\mathbf{e}_y, \tag{18}$$

where $k = 2\pi/L$. In Figs. 1(b) and 1(c) we show the comparison between the predicted (black circles) and the computed superadiabatic forces using SE and BD (solid

lines). The values of the response coefficients $\eta$ and $\chi$ [cf. (18)] have been adjusted to fit each amplitude; see the Supplemental Material [25] for details.

The theory then predicts the shape of both viscous and structural forces without further adjustable parameters, and it is in excellent agreement with the results from SE and BD. In addition, the linear (quadratic) scaling of the viscous (structural) force with the velocity [Fig. 2(a)] is also accounted by the theory [cf. (17)]. Because of the saturation of both superadiabatic forces [inset of Fig. 2(a)], it is necessary to analyze very small driving to obtain the correct scaling. Also, at low average density $\rho_0$ the viscous force is proportional to $\rho_0$ [see Fig. 2(b)], which according to (18) implies $\eta \propto \rho_0^2$, as expected [8]. See the Supplemental Material [25] for results for strong driving conditions and for a theoretical prediction of the density profile.

Memory plays a vital role in nonequilibrium systems, as we show in Fig. 2(c), by investigating the transient time evolution after switching on the driving at $t = 0$ [cf. (9)]. Both superadiabatic force contributions vanish in equilibrium ($t \leq 0$) and saturate in steady state ($t \to \infty$). At short times after switching on the driving force, the viscous (structural) force is linear (quadratic) in $t$, in full agreement with the non-Markovian form of (15). See the Supplemental Material [25] for an analysis of the scaling of the amplitude of the forces with wave number $k$. Here we have still taken $\mathbf{e}_v = \mathbf{e}_x$ as a (very good) approximation.

We conclude that the structural force is a primary candidate for a universal mechanism that leads to nonequilibrium structure formation. Examples of systems where a force acts perpendicular to the flow include shear banding [1–3], colloidal lane formation [4,5], and effective interactions in active spinning particles [29,30]. The theory that we present here operates in a self-contained way on the one-body level of correlation functions and hence is different from the approach of Refs. [7,11], where a dynamic closure on the two-body level via modeling of Brownian "scattering" is postulated. Note that the treatment of Refs. [7,11] relies on the density distribution as the fundamental variable; in contrast, our theory predicts the behavior of the system directly from the velocity field [cf. (16) and (17)].

We have focused here on the viscous and structural contributions to the superadiabatic force in shear-type flow. In compressional flow, where $\nabla \cdot \mathbf{v} \neq 0$, further force contributions can occur. Calculating the values for the transport coefficients $\eta$ and $\chi$ within the current theory is desirable, based, e.g., on the two-body level of correlation functions [31]. Furthermore, interesting research tasks for the future include investigating the effects of inhomogeneous temperature fields [32] and the possible emergence of time-periodic states ("time crystals" [33]) in inertial dynamics [34].

This work is supported by the German Research Foundation (DFG) via SCHM 2632/1-1.

N. C. X. S. and T. E. contributed equally to this work.

*delasheras.daniel@gmail.com; www.danieldelasheras.com
†Matthias.Schmidt@uni-bayreuth.de

[1] J. K. G. Dhont, Phys. Rev. E **60**, 4534 (1999).
[2] J. K. G. Dhont, M. P. Lettinga, Z. Dogic, T. A. J. Lenstra, H. Wang, S. Rathgeber, P. Carletto, L. Willner, H. Frielinghaus, and P. Lindner, Faraday Discuss. **123**, 157 (2003).
[3] H. Jin, K. Kang, K. H. Ahn, and J. K. G. Dhont, Soft Matter **10**, 9470 (2014).
[4] J. Chakrabarti, J. Dzubiella, and H. Löwen, Phys. Rev. E **70**, 012401 (2004).
[5] C. W. Wächtler, F. Kogler, and S. H. L. Klapp, Phys. Rev. E **94**, 052603 (2016).
[6] M. Krüger and J. M. Brader, Europhys. Lett. **96**, 68006 (2011).
[7] J. M. Brader and M. Krüger, Mol. Phys. **109**, 1029 (2011).
[8] J. Reinhardt, F. Weysser, and J. M. Brader, Europhys. Lett. **102**, 28011 (2013).
[9] A. A. Aerov and M. Krüger, J. Chem. Phys. **140**, 094701 (2014).
[10] A. A. Aerov and M. Krüger, Phys. Rev. E **92**, 042301 (2015).
[11] A. Scacchi, M. Krüger, and J. M. Brader, J. Phys. Condens. Matter **28**, 244023 (2016).
[12] J. Zausch, J. Horbach, M. Laurati, S. U. Egelhaaf, J. M. Brader, Th. Voigtmann, and M. Fuchs, J. Phys. Condens. Matter **20**, 404210 (2008).
[13] Ch. J. Harrer, D. Winter, J. Horbach, M. Fuchs, and Th. Voigtmann, J. Phys. Condens. Matter **24**, 464105 (2012).
[14] R. Ni, M. A. Cohen Stuart, and P. G. Bolhuis, Phys. Rev. Lett. **114**, 018302 (2015).
[15] U. Zimmermann, F. Smallenburg, and H. Löwen, J. Phys. Condens. Matter **28**, 244019 (2016).
[16] D. de las Heras, N. Doshi, T. Cosgrove, J. Phipps, D. I. Gittins, J. S. van Duijneveldt, and M. Schmidt, Sci. Rep. **2**, 789 (2012).
[17] B. Ruzicka, E. Zaccarelli, L. Zulian, R. Angelini, M. Sztucki, A. Moussad, T. Narayanan, and F. Sciortino, Nat. Mater. **10**, 56 (2011).
[18] M. Schmidt and J. M. Brader, J. Chem. Phys. **138**, 214101 (2013).
[19] A. Fortini, D. de las Heras, J. M. Brader, and M. Schmidt, Phys. Rev. Lett. **113**, 167801 (2014).
[20] D. de las Heras and M. Schmidt, Phys. Rev. Lett. **120**, 028001 (2018).
[21] See, e.g., A. J. Archer and R. Evans, Phys. Rev. E **64**, 041501 (2001); A. J. Archer, J. Phys. Condens. Matter **17**, 1405 (2005).
[22] W. H. Press, S. A. Teukolsky, W. T. Vetterling, and B. P. Flannery, *Numerical Recipes: The Art of Scientific Computing*, 3rd ed. (Cambridge University Press, Cambridge, England, 2007).
[23] E. Bernreuther and M. Schmidt, Phys. Rev. E **94**, 022105 (2016).
[24] D. de las Heras and M. Schmidt, Phys. Rev. Lett. **120**, 218001 (2018).
[25] See Supplemental Material at http://link.aps.org/supplemental/10.1103/PhysRevLett.121.098002 for descriptions of superadiabatic force profiles under strong driving conditions, scaling of the superadiabatic forces with the inverse box length, fitting details, and theoretical prediction of the density profile.
[26] R. Evans, Adv. Phys. **28**, 143 (1979).

[27] U. M. B. Marconi and P. Tarazona, J. Chem. Phys. **110**, 8032 (1999).
[28] A. J. Archer and R. Evans, J. Chem. Phys. **121**, 4246 (2004).
[29] N. H. P. Nguyen, D. Klotsa, M. Engel, and S. C. Glotzer, Phys. Rev. Lett. **112**, 075701 (2014).
[30] J. L. Aragones, J. P. Steimel, and A. Alexander-Katz, Nat. Commun. **7**, 11325 (2016).
[31] J. M. Brader and M. Schmidt, J. Chem. Phys. **139**, 104108 (2013); **140**, 034104 (2014); J. Phys. Condens. Matter **27**, 194106 (2015).
[32] For recent work, see, e.g., G. Falasco and K. Kroy, Phys. Rev. E **93**, 032150 (2016).
[33] J. Zhang *et al.*, Nature (London) **543**, 217 (2017); R. Moessner and S. L. Sondhi, Nat. Phys. **13**, 424 (2017).
[34] Power functional theory for quantum and for classical Newtonian dynamics is formulated, respectively, in M. Schmidt, J. Chem. Phys. **143**, 174108 (2015); **148**, 044502 (2018).